A New Approach of Arc Skeletonization for Tree-Like Objects Using Minimum Cost Path

Dakai Jin[1], **Krishna S Iyer**[2], **Eric A Hoffman**[2], and **Punam K Saha**[1,2]

[1]*Department of Electrical and Computer Engineering*, University of Iowa, Iowa City, USA

[2]*Department of Radiology*, University of Iowa Iowa City, USA

Abstract

Traditional arc skeletonization algorithms using the principle of Blum's transform, often, produce unwanted spurious branches due to boundary irregularities and digital effects on objects and other artifacts. This paper presents a new robust approach of extracting arc skeletons for three-dimensional (3-D) elongated fuzzy objects, which avoids spurious branches without requiring post-pruning. Starting from a root voxel, the method iteratively expands the skeleton by adding a new branch in each iteration that connects the farthest voxel to the current skeleton using a minimum-cost geodesic path. The path-cost function is formulated using a novel measure of local significance factor defined by fuzzy distance transform field, which forces the path to stick to the centerline of the object. The algorithm terminates when dilated skeletal branches fill the entire object volume or the current farthest voxel fails to generate a meaningful branch. Accuracy of the algorithm has been evaluated using computer-generated blurred and noisy phantoms with known skeletons. Performance of the method in terms of false and missing skeletal branches, as defined by human expert, has been examined using *in vivo* CT imaging of human intrathoracic airways. Experimental results from both experiments have established the superiority of the new method as compared to a widely used conventional method in terms of accuracy of medialness as well as robustness of true and false skeletal branches.

Keywords

Arc skeletonization; distance transform; geodesic distance; minimum cost path; airway tree

I. INTRODUCTION

Skeletonization [1-12] provides a simple yet compact representation of an object that has widely been used in a variety of applications from computer vision, pattern recognition, and medical imaging [13, 14]. For three-dimensional (3-D) objects, two different types of skeletonization method, namely surface skeletonization and curve or arc skeletonization, have been popularly applied depending upon the geometry of target objects and the purpose of an application. Surface skeletonization generates a medial representation of an object,

dakai-jin@uiowa.edu. punam-saha@uiowa.edu. krishna-iyer@uiowa.edu. eric-hoffman@uiowa.edu.

which is a union of finitely many surfaces and curves each being symmetrically placed in the object. Surface skeletonization has been used in many applications including thickness computation [15, 16], local structure characterization [17, 18] etc.

This paper deals with arc skeletonization of 3-D tree-like elongated objects, e.g., vascular or airway trees; here, we use the term "arc skeletonization" instead of "curve skeletonization". Arc skeletonization is primarily used for elongated objects, which generates a centerline representation as a union of finitely many curves. In the literature, there exist a large number of arc skeletonization methods [19-21] for elongated 3-D objects. Generally, these methods fall under two categories - topology preserving iterative erosion [6-8, 22, 23] or distance transform based technique [2, 5, 9, 24]. Although these methods generate an arc skeleton with the same object topology and elongatedness, often, a large number of spurious or false branches and jagged curves are produced by such methods. Therefore, many researchers have suggested post-processing algorithms to prune and beautify resulted arc skeletons [2, 5, 18, 25-27]. However, even with skeletal pruning and beautification steps, resulted skeletons are inevitably left with some spurious or false branches caused by irregularities in object boundaries, noise, and other artifacts. Some methods [27] are effective in 2-D while their generalization to 3-D are not straightforward.

In this paper, we present a new arc skeletonization method that is different from Blum's grassfire principle [3], commonly used by conventional algorithms. The method starts with a root voxel as the seed skeleton and iteratively expands it by adding a new branch in each iteration that joins the farthest object voxel to the current skeleton using a minimum-cost geodesic path. The new method is robust in terms of suppressing spurious or false branches while capturing all meaningful branches. Another major advantage of the methods is that the same fundamental principle is equally applicable to both binary and fuzzy representations of an object. The performance of the method has been evaluated on computer-generated phantoms with known skeletons as well as on *in vivo* CT images of human intrathoracic airways. Computer generated phantoms at different down-sampling rates and additive Gaussian noise have been used to examine the method's accuracy in terms of agreement with known skeletons. CT image data of human intrathoracic airway tree is used to evaluate the method's performance in terms of false and missing branches. Principles and definitions of methods and algorithms are presented in Section II while the experimental design and results are described in Section III. Finally, the conclusion is drawn in Section IV.

II. Methods and algorithms

Description of methods and algorithms of the new arc skeletonization approach are presented in this section. Basic principles of the overall method are described in Section II.A using schematic illustrations. Three major steps, namely, skeletal branch detection, object volume filling, and termination criterion, are described in Section II.B, II.C, and II.D, respectively.

A. Basic principle

Conventional arc skeletonization algorithms are designed on the principle of Blum's grassfire transform implemented using some form of a voxel peeling approach that is

constrained by preservation of local topology and "elongatedness". This intrinsic strategy of using local properties for voxel peeling limits the utility of larger contextual information in conventional algorithms. Therefore, these methods suffer from irregularities in object boundaries and structure noise, e.g., the small protrusion p_{noise} in Fig. 1. The new method is designed for 2-D or 3-D tree-like objects with elongated branches (e.g., vascular or airway trees), which geodesic path from o to p_1 (see Fig. 1a). An important issue in this context is that the cost function should be chosen such that minimum-cost path passes through the centerline of the structure and a high cost is applied when it deviates from the centerline. After the skeletal branch op_1 is constructed, the representative object volume is filled by a local scale-adaptive dilation along the branch as shown in Fig. 1b. During the next iteration, the farthest geodesic point (here, p_2) is sought from the filled object volume and the skeleton is augmented by another branch op_2 joining p_2 to the current skeleton. This process continues until dilated skeletal branches fill the entire object volume or all meaningful branches have been found.

One important feature of the new method is that meaningfulness of individual skeletal branches are determined from their global context and, therefore, the method offers enhanced robustness in stopping noisy branches. Minimum-cost paths improve smoothness of skeletal branches. Also, depending upon the application, the initial root point may be automatically detected, e.g., (1) the point with the largest distance transform value, (2) the topmost point in the airway tree etc. Major components of the algorithm in a digital grid are presented in the following.

- Identify a root voxel as the initial skeleton and set it as the current filled object volume

- Iteratively perform the following steps until dilated skeletal branches fill the entire object volume or all meaningful branches have been found

- Find the farthest geodesic voxel from the current filled object volume

- If the farthest voxel is sufficiently far (geodesic distance) from the filled object volume, i.e., a meaningful branch may be derived then find the minimum-cost path joining the farthest voxel to the current skeleton

- Dilate the newly generated branch to augment the current filled object volume

Finally, it may be mentioned that surplus voxels are generated at a T-junction when a branch is created. It is solved by deleting non-arc-end 3-D simple points [10].

In the following sections, different components of the algorithm are described in details. In this paper, the *cubic image grid* Z^3, where Z is the set of integers, is used and an element $p \in Z^3$ of the grid is referred to as a *voxel*. A *fuzzy digital object* is defined as a fuzzy subset of Z^3 and is denoted as $O = \left\{ (p, \mu_O(p)) | p \in Z^3 \right\}$ where $\mu_o : Z^3 \rightarrow [0,1]$ is the *membership function*. The *support* of a fuzzy object, denoted as O, is the set of voxels with non-zero membership values, i.e., $O = \left\{ p | p \in Z^3 \wedge \mu_O(p) \neq 0 \right\}$. A voxel inside the support of an object is referred to as an *object voxel*.

B. Skeletal branch detection

During an iteration, the skeleton is expanded by exactly one meaningful skeletal branch. The first task is to find the farthest geodesic voxel from the filled object volume for which a skeletal branch has already been found. This task is accomplished by binary distance transform (DT) [30, 31] or fuzzy distance transform (FDT) [32] from the filled volume and then selecting the voxel with the largest DT or FDT value.

The next task is to connect the farthest voxel to the current skeleton by a smooth branch that also runs along the centerline of the object. As mentioned earlier, the new branch is selected as the minimum-cost geodesic path. To impose medialness of the branch, the path is encouraged to pass through centers of maximal balls (CMB) [5, 33]. However, such CMBs are highly sensitive to noise, especially, for fuzzy objects. To further improve the performance, a measure of local significance factor (LSF) [5], which is a measure of impulse by opposing fire-fronts, is used to define path cost. LSF at an object voxel $p \in O$ in a fuzzy object O is defined as follows:

$$LSF(p) = 1 - f_+ \left(max_{q \in N^*(p)} \frac{FDT(q) - FDT(p)}{\frac{1}{2}(\mu_o(p) + \mu_o(q))|p - q|} \right), \quad (1)$$

where the function $f_+(x)$ returns the value of x if $x > 0$ and zero otherwise; and $N^*(p)$ is the 26-neighborhood of p. It can be shown that LSF at a CMB lies in the interval $(0,1]$ and it takes the '0' value at non-CMB voxels.

LSF measure is used to define path cost. A *path* π is an ordered sequence of voxels where every two successive voxels are 26-adjacent, i.e., $\pi = \langle p_0, p_1, \cdots, p_{l-1} \rangle$ where $p_{i-1}, p_i \in Z^3$ are 26-adjacent for every $i = 1, \ldots, l - 1$. Total path cost is defined by adding the cost of individual discrete steps between every two successive voxels on the path. The step-cost of a discrete step between two 26-adjacent voxels $p, q \in Z^3$ is defined as follows:

$$SC(p, q) = \frac{|p - q|}{1 + \alpha(min(LSG(p), LSF(q)))^n}, \quad (2)$$

where the two parameters α and n determine the trade-off between the smoothness and medialness of the minimum-cost path. A higher weight of LSF value in the step-cost function leads to more medialness while a lower weight of LSF value generates straighter paths. In this paper, the values of α and n are chosen as '1' and '2', respectively. Results of LSF values and the step-cost map are illustrated in Fig. 3c,d, respectively.

The cost of a path $\pi = \langle p_0, p_1, \cdots, p_{l-1} \rangle$ denoted as *Cost*(π), is computed as the sum of the costs of individual steps on the path, i.e.,

$$Cost(\pi) = \sum_{i=1}^{l-1} SC(p_{i-1}, p_i). \quad (3)$$

As stated earlier, our objective is to join the farthest geodesic object voxel to the current skeleton by a new skeletal branch. Let p be the farthest geodesic object voxel and let S

denote the current skeleton. The branch $BR_{S,p}$ joining the skeleton S and the farthest object voxel p is defined as the minimum cost path

$$BR_{S,p} = arg \min_{\pi \in \Pi_{S,p}} Cost(\pi), \quad (4)$$

where $\Pi_{s,p}$ is the set of all possible geodesic paths between the skeleton and the voxel p. The minimum-cost path $BR_{S,p}$ may be computed using a dynamic programming algorithm. It may be noted that, although, a dynamic programming algorithm always generates a minimum-cost path, the minimum-cost path between a set of voxels and another voxel is not necessarily unique. Cross-sections of minimum-cost paths representing different skeletal branches on a 2-D image slice are shown in Fig. 3e.

C. Object volume filling

The final step during an iteration is to fill the object volume represented by a newly added skeletal branch. After finding the minimum-cost path, a local volume filling operation is applied along the new branch path $BR_{S,p}$. This step helps avoiding spurious or false branches, especially, at object regions with large scales, for example, at trachea of intrathoracic airway tree. A local scale-adaptive volume-filling algorithm is applied to fill the object volume represented by a newly added branch. It is implemented using a modified FDT algorithm. Local scale of dilation $scale(q)$ at a given voxel q on $BR_{S,p}$ is defined as follows:

$$scale(q) = (1+K)FDT(q). \quad (5)$$

In the above equation, the parameter K is a positive value which is used to ensure that the local object region is completely filled by dilation. It may be noted that some extra filling does not negatively influence the results; rather, it helps stopping some noisy braches. In this paper, the value of the parameter K is chosen as '1'. The dilation process is implemented as follows. At every voxel q on $BR_{S,p}$, the FDT value is initialized as - $scale(q)$, the negative value of its dilation scale. Then FDT is computed within the support of the object using dynamic programming and, finally, the regions with negative or zero FDT values are filled. Results of filling on an image slice are shown in Fig. 3f.

D. Termination critierion

The algorithm iteratively adds skeletal branch and it terminates when either of the following two conditions are fulfilled - (1) the entire object region is entirely filled, or, (2) the geodesic distance of the next farthest voxel from the object volume filled by the current skeleton is not large enough. The first condition indicates that the entire object volume has already been filled by skeleton branches and no further skeletal branch may be added. The second condition indicates that no more meaningful skeletal branch may be added. In this paper, a distance threshold of three voxels is used for the farthest voxel. In this context, it must be mentioned that, since the geodesic distance of the farthest voxel is computed from filled object volume, the length of the branch does not define meaningfulness of a branch. At large-scale object regions, it is possible to visualize a situation where a branch may be long enough while failing to become a meaningful one. In such a situation, major portion of the

branch falls inside the object region already filled by representative skeletal branches. Final results of skeletonization for a CT-based human intrathoracic airway tree are shown in Fig. 2c. As it appears visually, the algorithm successfully traces all true branches while stopping false branches.

III. Experiments and results

Two experiments were carried out to quantitatively examine the performance of the proposed method and to compare it with a conventional algorithm. Here, we have chosen the arc-skeletonization algorithm by Palágyi *et al.* [34] for comparison which has been popularly used for airways. Also, the algorithm by Palágyi *et al.* uses a post-pruning step to remove noisy branches. The first experiment was designed using computer-generated airway phantoms with known centerlines to examine the accuracy of the method in terms of agreement of computed skeleton with known centerlines. The second experiment was conducted on clinical CT data of human intrathoracic airway trees to evaluate the performance of the method in terms of false and missing branches as marked by a human expert. These experiments and observed results are described in the following sections.

A. Accuracy of arc skeletonization

To quantitatively examine the accuracy of the method, one human airway tree phantom with known centerlines was generated at each of three different levels of down-sampling and three different levels of noise (Fig. 4b-d). These phantoms were generated in the following steps - (1) segmentation of airway lumen using a region growing algorithm [35], (2) arc skeletonization [11] and computation of local airway lumen thickness [15], (3) pruning of arc skeleton beyond the 6th anatomic level of branching, (4) up-sampling of the skeleton and local thickness map by 2×2×2 voxels, (5) fitting of a B-spline to each individual skeletal branch, (6) smoothing thickness values along each skeletal branch, (7) reconstruction of a smooth airway tree volume using local thickness-adaptive dilation along each skeletal branch, (8) down-sampling of known centerline and corresponding airway volume at 3×3×3, 4×4×4, and 5×5×5 voxels, (9) addition of zero-mean correlated white Gaussian noise at a signal-to-noise ratio of 24, 12, and 6.

Results of arc skeletonization for an airway phantom (Fig. 4a) at three different levels of down-sampling and three different levels of noise (Fig. 4b-d) are shown in Fig. 4e-g. Skeletonization error was calculated by comparing computed and true skeletons. True skeleton was generated by sampling the B-spline based skeletal branches in the continuous 3-D space R^3. Let S_T be the set of N_T number of sample points in a true skeleton. Let $S_C^{l,\rho}$ denote the computed skeleton by a given method at the down-sampling rate of F and the noise at SNR of ρ and let $N_C^{l,\rho}$ denote the number of voxels in $S_C^{l,\rho}$ Skeletonization error was computed as follows:

$$Error_{l,\rho} = \frac{1}{2N_T} \sum_{p \in S_T} \min_{q \in S_C^{l,\rho}} |p - q| + \frac{1}{2N_C^{l,\rho}} \sum_{p \in S_C^{l,p}} \min_{q \in S_T} |p - q|. \quad (6)$$

Average errors for phantoms at different levels of down-sampling and noise are presented in Table 1. At each level of downsampling and noise, the average error using the new algorithm (Table 1a) is less than that by Palágyi et al.'s algorithm. As shown in the table, the average error is less than a voxel and as discussed by Saha *et al.* [16], the average digitization error is close to 0.38 voxel. Therefore, after deducting the digitization error, the performance of the new algorithm even at the highest level of noise and down sampling is very encouraging. Also, it may be noted that, at a given down sampling rate, the performance of our method is almost insensitive to noise. The primary reason behind this strong performance is that the new method detects a significant branch using path integral of a cost function and the effects of noise is significantly reduces by the path-integration.

B. Evaluation of false and missing branches

To evaluate the performance of the method in terms of false and missing branches, five human pulmonary CT images were used and the analysis was performed on airway tree skeletonization. These images were acquired on a Siemens Sensation 64 multi-row detector CT scanner using the following protocol: 120 kV, 100 effective mAs, pitch factor: 1.0, nominal collimation: 64×0.6mm, image matrix: 512×512 and $(0.55 \text{ mm})^2$ in-plane resolution. Airway trees were segmented using a region growing algorithm and granular noisy protrusion and dents were added on airway border. It was ensured that the dents and protrusions do not create any cavities and tunnels [29]. Results of application of the new method and the algorithm by Palágyi *et al*. are shown in Fig. 5. The new method successfully stopped noisy branches for most noisy granulates on the airway border except for a few locations as shown in a zoomed panel on the left. On the other hand, Palágyi *et al*.'s algorithm produced undesired branches at many noisy protrusions. Both algorithms successfully detected all visible branches. To quantitatively examine the performance of the two methods, one expert observer visually labeled false and missing braches up to fifth generation of airway tree. The original airway tree prior to addition of noise was used for labeling noisy and missing branches. Following the expert observer, both methods successfully preserved all true branches in computed arc skeletons. Based on the expert observer's labeling on five nosy airway trees, the new method produced an average of 2.4 false branches on each airway tree while Palágyi *et al*.'s algorithm produced an average of 31.4 false branches. The maximum number of false branches by the new method for any image used in this experiment was five.

IV. Conclusion

A new approach of computing arc-skeleton for three-dimensional tree-like objects has been presented and its performance has been evaluated. The new method uses an initial root seed voxel to grow the skeleton. A novel path-cost function has been designed using a measure of local significance factor, which forces new branches to adhere to the centerline of an object. The method uses global contextual information while adding a new branch, which contributes additional power to stop false or noisy branches. Quantitative evaluative experiments on realistic phantoms with known centerlines have demonstrated that the new method is more accurate than a popular conventional method. The other experiment using airway tree data with additional noisy dents and protrusions has shown that the new method

significantly reduces the number of noisy or false branches as compared to a conventional algorithm. In this paper, a threshold on geodesic distance of the farthest voxel from object volume filled by representative skeletal branches is used to determine meaningfulness of a new branch. Currently, we are working on defining a scale-adaptive smart criterion to define meaningfulness of a skeletal branch. One concern of the new method is high computational complexity. At present, we are developing a computationally efficient algorithm that exploits the volumetric sparseness of object voxels in a tree-like structure and that will minimize repetitive computation of FDT, path-cost, farthest geodesic voxel, and volume filling.
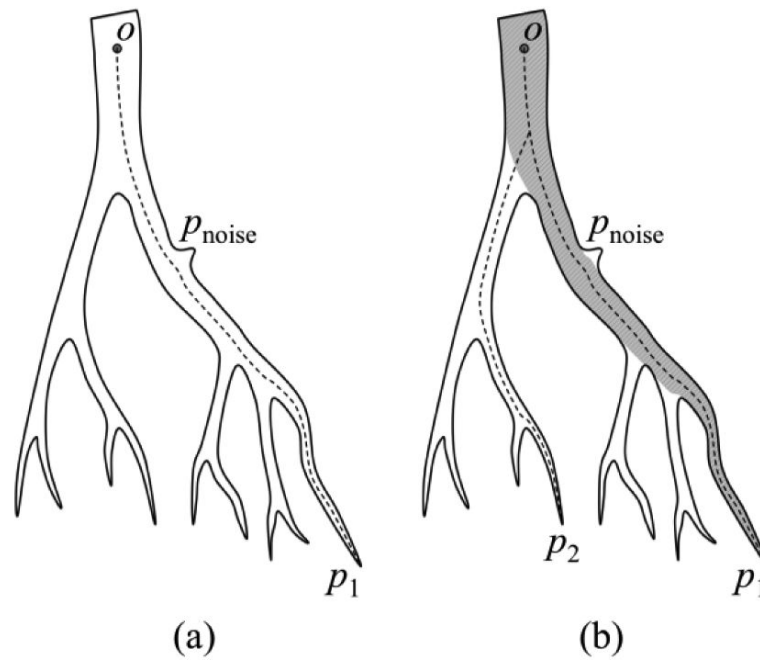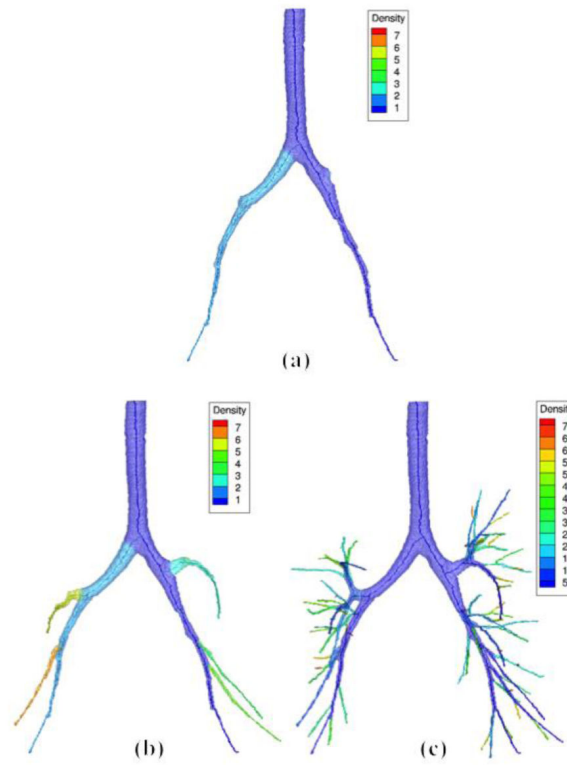
Acknowledgment

REFERENCES

[1]. Arcelli C, Sanniti di Baja G. A width-independent fast thinning algorithm. IEEE Trans Pattern Anal Mach Intell. 1985; 7:463–474. [PubMed: 21869284]

[2]. Arcelli C, Sanniti di Baja G, Serino L. Distance-driven skeletonization in voxel images. IEEE Trans Pattern Anal Mach Intell. 2011; 33:709–720. [PubMed: 20714012]

[3]. Blum H. A transformation for extracting new descriptors of shape. Models for the perception of speech and visual form. 1967; 19:362–380.

[4]. Borgefors G, Nyström I, Sanniti di Baja G. Computing skeletons in three dimensions. Pattern Recognition. 1999; 32:1225–1236.

[5]. Jin, D.; Saha, PK. A new fuzzy skeletonization algorithm and its applications to medical imaging; 17th International Conference on Image Analysis and Processing (ICIAP); Naples, Italy. 2013. p. 662-671.LNCS

[6]. Lee T-C, Kashyap RL, Chu C-N. Building skeleton models via 3-D medial surface/axis thinning algorithm. CVGIP: Graphical Models and Image Processing. 1994; 56:462–478.

[7]. Ma CM, Sonka M. A fully parallel 3D thinning algorithm and Its applications. Computer Vision Image Understanding. 1996; 64:420–433.

[8]. Palágyi K, Kuba A. A parallel 3D 12-subiteration thinning algorithm. Graphical Models and Image Processing. 1999; 61:199–221.

[9]. Pudney C. Distance-ordered homotopic thinning: a skeletonization algorithm for 3D digital images. Computer Vision and Image Understanding. 1998; 72:404–413.

[10]. Saha PK, Chaudhuri BB. Detection of 3-D simple points for topology preserving transformations with application to thinning. IEEE Transactions on Pattern Analysis and Machine Intelligence. 1994; 16:1028–1032.

[11]. Saha PK, Chaudhuri BB, Dutta Majumder D. A new shape preserving parallel thinning algorithm for 3D digital images. Pattern Recognition. 1997; 30:1939–1955.

[12]. Tsao YF, Fu KS. A parallel thinning algorithm for 3D pictures. Computer Graphics and Image Processing. 1981; 17:315–331.

[13]. Saha, PK. International Conference on Pattern Recognition and Machine Intelligence. Indian Statistical Institute; Kolkata, India: 2013. Fuzzy digital topology and geometry and their applications to medical imaging.

[14]. Saha PK, Strand R, Borgefors G. Digital topology and geometry in medical imaging: a survey. IEEE Transactions on Medical Imaging. submitted.

[15]. Liu Y, Jin D, Li C, Janz KF, Burns TL, Torner JC, Levy SM, Saha PK. A robust algorithm for thickness computation at low resolution and its application to in vivo trabecular bone CT imaging. IEEE Transactions on Biomedical Engineering. 2014 in press.

[16]. Saha PK, Wehrli FW. Measurement of trabecular bone thickness in the limited resolution regime of in vivo MRI by fuzzy distance transform. IEEE Transactions on Medical Imaging. 2004; 23:53–62. [PubMed: 14719687]

[17]. Saha PK, Gomberg BR, Wehrli FW. Three-dimensional digital topological characterization of cancellous bone architecture. International Journal of Imaging Systems and Technology. 2000; 11:81–90.

[18]. Saha PK, Xu Y, Duan H, Heiner A, Liang G. Volumetric topological analysis: a novel approach for trabecular bone classification on the continuum between plates and rods. IEEE Trans Med Imaging. 2010; 29:1821–38. [PubMed: 20562041]

[19]. Greenspan H, Laifenfeld M, Einav S, Barnea O. Evaluation of center-line extraction algorithms in quantitative coronary angiography. IEEE Transactions on Medical Imaging. 2001; 20:928–941. [PubMed: 11585209]

[20]. Sonka M, Winniford MD, Zhang X, Collins SM. Lumen centerline detection in complex coronary angiograms. IEEE Trans Biomed Eng. 1994; 41:520–8. [PubMed: 7927371]

[21]. Wang S, Wu J, W M, Ma X. Robust curve skeleton extraction for vascular structures. Graphical Models. 2012; 74:109–120.

[22]. Sadleir RJT, Whelan PF. Fast colon centreline calculation using optimised 3D topological thinning. Computerized Medical Imaging and Graphics. 2005; 29:251–258. [PubMed: 15890252]

[23]. Xie W, Thompson RP, Perucchio R. A topology-preserving parallel 3D thinning algorithm for extracting the curve skeleton. Pattern Recognition. 2003; 36:1529–1544.

[24]. Serino L, Arcelli C, Sanniti di Baja G. On the computation of the <3,4,5> curve skeleton of 3D objects. Pattern Recognition Letters. 2010; 32:1406–1414.

[25]. Attali D, Sanniti di Baja G, Thiel E. Skeleton simplification through non significant branch removal. Image Processing and Communications. 1997; 3:63–72.

[26]. Shaked D, Bruckstein AM. Pruning Medial Axes. Computer Vision and Image Understanding. 1998; 69:156–169.

[27]. Bai X, J. Latecki L, Liu WY. Skeleton pruning by contour partitioning with discrete curve evolution. IEEE Trans Pattern Anal Mach Intell. 2007; 29:449–62. [PubMed: 17224615]

[28]. Saha PK, Chaudhuri BB, Chanda B, Dutta Majumder D. Topology preservation in 3D digital space. Pattern Recognition. 1994; 27:295–300.

[29]. Saha PK, Chaudhuri BB. 3D digital topology under binary transformation with applications. Computer Vision and Image Understanding. 1996; 63:418–429.

[30]. Borgefors G. Distance transform in arbitrary dimensions. Computer Vision Graphics Image Processing. 1984; 27:321–345.

[31]. Borgefors G. Distance transformations in digital images. Computer Vision Graphics and Image Processing. 1986; 34:344–371.

[32]. Saha PK, Wehrli FW, Gomberg BR. Fuzzy distance transform: theory, algorithms, and applications. Computer Vision and Image Understanding. 2002; 86:171–190.

[33]. Arcelli C, Sanniti di Baja G. Well-shaped, stable, and reversible skeletons from the (3,4)-distance transform. Journal of Visual Communication and Image Representation. 1994; 5:107–115.

[34]. Palágyi, Kálmán; Tschirren, Juerg; Hoffman, Eric A.; Sonka, Milan. Quantitative analysis of pulmonary airway tree structures. Computers in Biology and Medicine. 2006; 36:974–996. [PubMed: 16076463]

[35]. Saha PK, Udupa JK, Odhner D. Scale-based fuzzy connected image segmentation: theory, algorithms, and validation. Computer Vision and Image Understanding. 2000; 77:145–174.
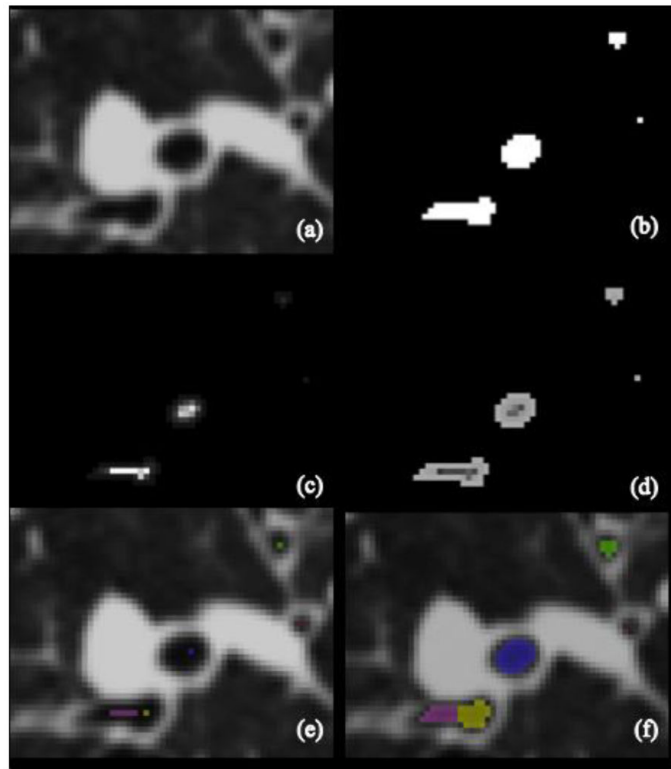
Fig. 1.
Schematic illustration of the new method. (a) The method starts with the rood point o as the initial skeleton and finds the farthest geodesic point p_1. This farthest point is connected to the skeleton by a new branch op_1 using a minimum-cost geodesic path. (b) The object volume corresponding to the current skeleton is filled and the next farthest geodesic point p_2 is found and another skeletal branch op_2 is added. It may be noted that the noisy protrusion p_{noise} does not create any noisy branch even after all meaningful branches are added to the skeleton.
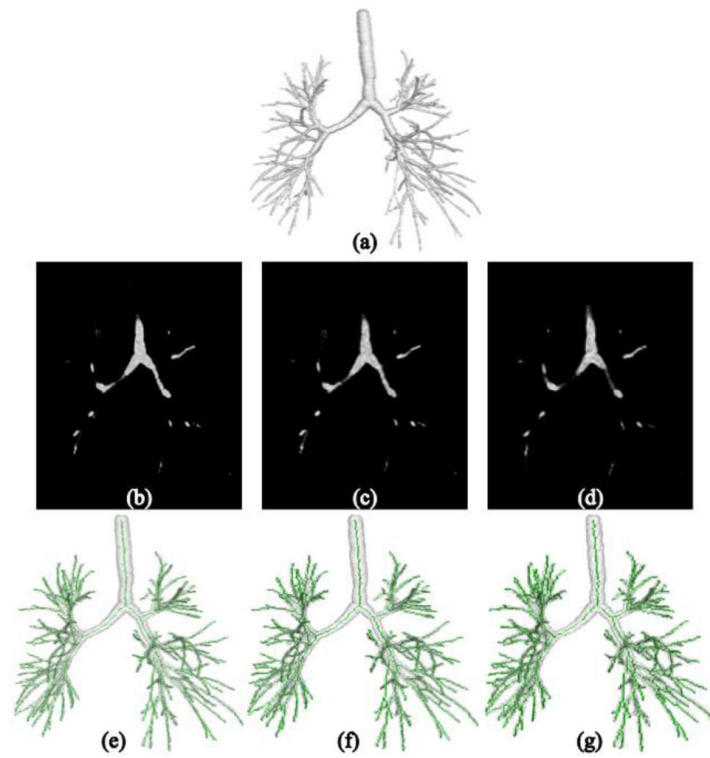
Fig. 2.
Results of arc skeletonization at different stages of skeletal expansion by the new method.
(a) The first two skeletal branches and corresponding filled object volume on CT image data
of a human intrathoracic airway tree. Filled object volumes by different branches are
rendered in different colors. (b,c) Same as (a) but after extracting more branches (b) and at
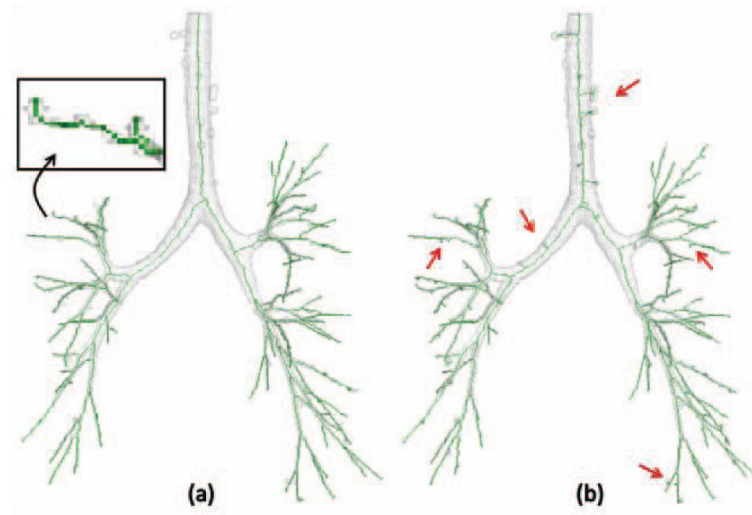the terminal condition (c).

Fig. 3.
Illustration of local significance factor and different cost functions on a small region in a 2-D image slice of a pulmonary CT image. (a) A small region from an original CT image slice. (b) Segmented airway lumen mask. (c,d) LSF (c) and path cost (d) functions. (e) Extracted centerlines. (f) Filleted object volume for different skeletal branches.

Fig. 4.
Results of arc skeletonization on phantom images at different levels of noise and down sampling. (a) 3D rendition of the original phantom. (b-d) Sagittal image slices at SNR of 24, 12 and 6 and down sampling of three, four, and five voxels. (e-g) Arc skeletons for the images of (b-d), respectively, using by the proposed method.

Fig. 5.
3D display of arc skeletonization of a CT-derived human intrathoracic airway tree after adding noisy protrusions and dents. The arc skeleton obtained by the new method (a) has significantly reduced false branches as compared to Palágyi algorithm (b). A zoomed in pane is shown in (a) to demonstrate a false branch by the new method. Both methods have successfully captured all visible meaningful branches.

Table 1

Arc skeletonization errors using the new method (a) and the algorithm by Palágyi *et al.* [34] (b). Each cell presents the mean and the standard deviation of skeletonization errors in voxel unit of corresponding down-sampled resolution.

down-sampling	Different signal to noise ratio		
	SNR 24	SNR 12	SNR 6
3×3×3	0.66±0.38	0.67±0.38	0.67±0.37
4×4×4	0.69±0.33	0.69±0.35	0.69±0.34
5×5×5	0.72±0.40	0.75±0.38	0.72±0.38

(a)

down-sampling	Different signal to noise ratio		
	SNR 24	SNR 12	SNR 6
3×3×3	0.78±0.39	0.78±0.40	0.79±0.40
4×4×4	0.86±0.43	0.86±0.41	0.86±0.41
5×5×5	0.92±0.39	0.92±0.40	0.92±0.40

(b)